



Emerging Science Journal

Vol. 4, No. 3, June, 2020



Altering Perceptions, Visualizing Sub-ground Metal Objects

Aleksander Pedersen ^{a*}^a Department of Computer Science and Computational Engineering, UiT The Arctic University of Norway, Narvik, Norway

Abstract

Smart phones and sensor technology represent a key part of everyday life and are being used in areas such as safety, training, healthcare and others. Utilizing an array of internal sensors and a metal detector requires an evaluation of the precision of the measurements and performance reviews. Metal detectors are versatile, with uses in healthcare as well as recreational, but a common issue often seen in the proprietary equipment is bad presentation of data. Usually the user interface is just numbers on a display, simplified graphs or sounds. By combining smartphone sensors with a metal detector and a custom mount we model a mapping between the virtual and physical model, a digital twin. In this paper we are utilizing the computing capabilities of a smartphone and employing visualization techniques not possible by partial information. In addition, we present an improved graphical user interface without any proprietary accessories. For this purpose, preliminary case studies are included as a part of a prototype in development.

Keywords:

Smartphone;
Metal Detector;
Digital Twin;
Visualization Technique;
Mapping.

Article History:

Received:	24	February	2020
Accepted:	02	May	2020
Published:	01	June	2020

1- Introduction

What we see in the recent years is an increased usage of sensors and sensor technology in all parts of life. For instance smart technology (houses and cities), health care applications [1] where among others, actuators and advanced communication technologies have created environments in patients home without the need of expensive healthcare facilities [2] and rehabilitation of patients [3], tracking and industry [4], and monitoring in sports applications [5]. A metal detector is a versatile device, with uses ranging from recreational to healthcare and food industry as well as robotics. Finding foreign metallic particles in food products [6] is crucial for good quality and better food safety assurance. Searching for foreign metallic objects for Ingestion in pediatric emergency [7] and in advanced robotics using Bluetooth to control a metal detector robot [8]. The most common device is the smart phone, with many applications utilizing the different built in sensors, some of which are used for exercising, gaming, etc. Another application area is to use external devices connected to the smart phone. In this work we combined the common sensors of a smart phone with the applications of a metal detector. To the best of our knowledge, there are no commercially available applications connecting an external metal detector to a mobile phone. What already exists are very specific and proprietary products. The provided simple user interfaces such as display, or headphones connected by Bluetooth or cable are optional accessories. By expanding the magnetic information collected by a search coil, with geometry from sensor information such as compass, gyro and accelerometer, we can generate informative plots that provide insight not gained from search coil sounds and classification alone.

The main purpose of this work is to construct a custom hybrid setup which combines the standard output of a metal detector with the sensors and computing capabilities of off-the-shelf smartphones, into simple algorithms which can replace today's proprietary solutions. A secondary part has been to find a way to visualize the data on a smartphone screen concisely.

* CONTACT: Aleksander.pedersen@uit.no

DOI: <http://dx.doi.org/10.28991/esj-2020-01224>

© 2020 by the authors. Licensee ESJ, Italy. This is an open access article under the terms and conditions of the Creative Commons Attribution (CC-BY) license (<https://creativecommons.org/licenses/by/4.0/>).

From the tools available today we know that improvements can be made, and especially on the presentation given by the metal detector setup. The presentation is usually just numbers on a display, some simplified graphs or a sound (pitch) stating the depth and type of material reflected.

Combination of information can be used to either provide new insights not possible by partial information or make a toolset that make certain operations easier.

2- Components

The two main components of the custom setup are the metal detector and a smartphone. The smartphone is presumed attached to the metal detector in a fixed orientation. Throughout this work we consider the mount fixed along the handle of the metal detector with the screen pointing up towards the user. Additionally, the smartphone frame is considered fixed with respect to the search area plane, see Figure 1.

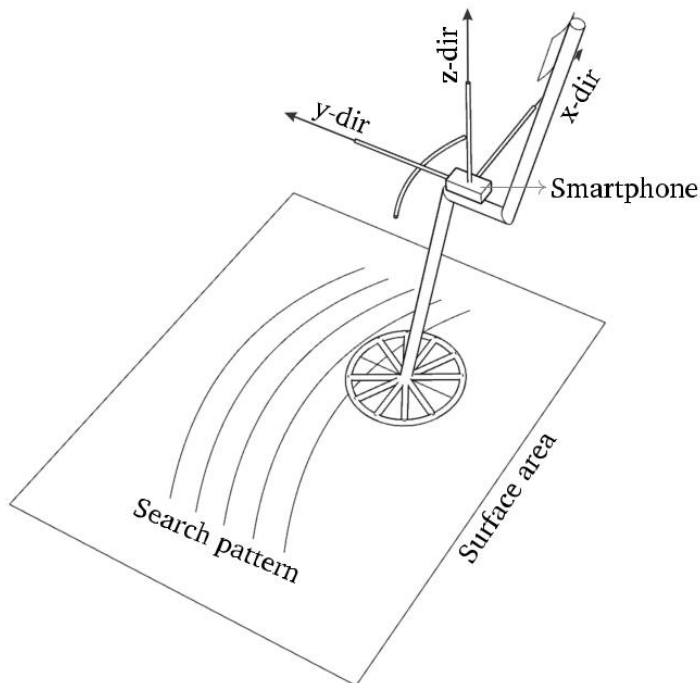


Figure 1. Illustration of the custom mount attaching the phone to the metal detector with the axes aligned with the metal detector frame.

2-1- Metal Detector

In principle the functional parts of a metal detector consist of two coils, a search coil and a detector coil and a set of control logic. The search coil generates an electromagnetic field, and the detector receives the replicated field generated by the metallic objects, Eddy current [9]. The output from the metal detector is then transferred to the control logics which emit an audio signal indicating the type of material. The audio signal can then be recorded and used for the purpose of analysis.

2-2- Smartphone Components

The metal detector has its own control logic, and by adding an extra layer of information using built in sensors such as:

- Accelerometer
- Gyroscope
- Rotation vector (attitude composite sensor)
- Microphone

For the simplest motion-based representation, the accelerometer is used to detect movement changes in x, y, and z-axis. The gyroscope is used for orientation by measuring the rate of rotation for the three-coordinate axis. The rotation vector is an attitude composite sensor reporting the orientation relative to an East-North-Up coordinate frame by integrating the underlying accelerometer, magnetometer and gyroscope readings. The microphone has its own reporting mechanism which can be invoked using the android library.

2-3- Frame Representation

The metal detector and smartphone are modeled as a digital twin, where the smartphone orientation is represented using a spatial 3-component frame following a right-hand system [10]. The phone frame is fixed, that is, the z-axis is aligned with the detector pointing upwards. The y-axis is aligned with the forward direction of the handle. The x-axis is orthogonal to the y- and z-axis, pointing towards the right.

3- Digital Twin

To calibrate the smartphone sensors, we utilize an experiment which calibrates the phone sensors with an approximated pendulum motion. The x-axis is deciding the search pattern going from side to side when sweeping the metal detector over a surface area. The commercial device is replaced by a custom prototype based on a smart phone. The metal detector is a DEUS XP Metal detector [11]. The custom mount is a Celestron NEXYZ 3-AXIS Universal Smartphone Adapter [12].



Figure 2. Setup from the side



Figure 3. Setup from the front

4- Results

The sound emitted from the metal detector is recorded on the smart phone and analyzed by performing frequency analysis. From this we can say something about the object or objects that are in the scope of the metal detector. The plot of a raw audio sample is shown in Figure 4.

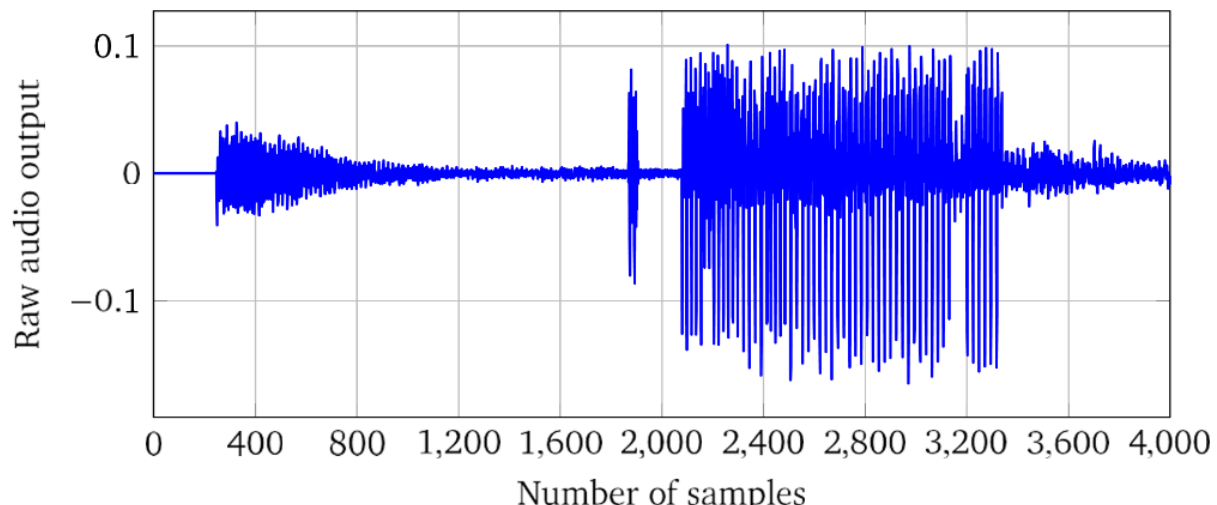


Figure 4. Raw output from the metal detector using the phone as a recording device.

The audio was sampled using a part of the android API called `AudioRecord`. `AudioRecord` is configured to use a 16-bit mono channel at a frequency of 12kHz. This audio data is then being processed using Fast Fourier transform (FFT). The result is a multi-resolution analysis with equally distributed bands of 256 samples.

Distributed over the whole spectrum, this gives $\frac{12000\text{Hz}}{256\text{Samples}} = 46,875\text{ Hz/Sample}$. We can now compute the frequency for each amplitude in the graph, seen in Figure 5. By using the mapping from sample index to frequency as we described above, the "beep" signal sound from the metal detector can be detected.

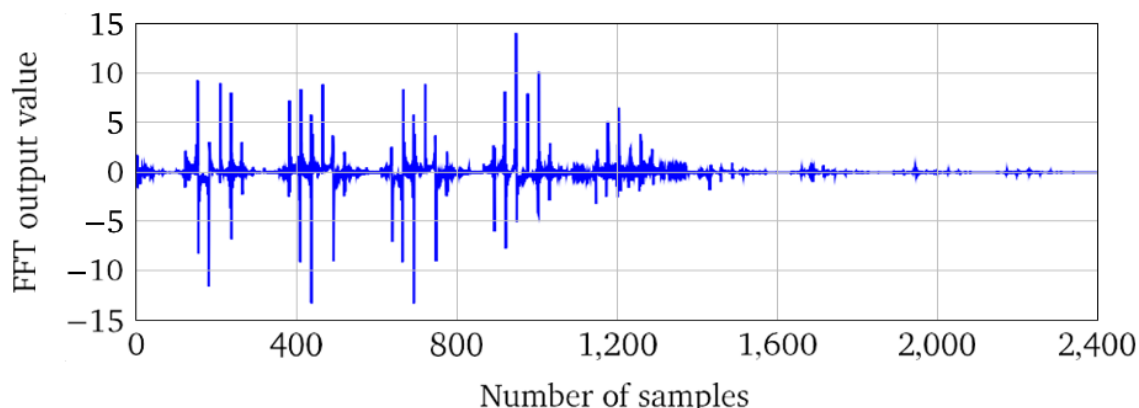


Figure 5. The graph presented here is the FFT processed audio from a recorded session using the sound output from the metal detector.

Two bands are illustrated in Figure 6, showing a specific pattern emitted (left-hand side) and a signal containing noise only (right-hand side).

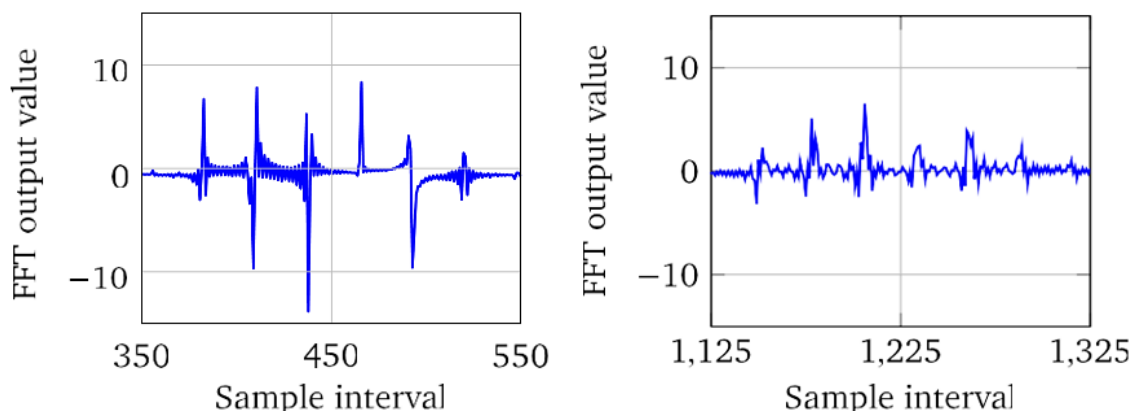


Figure 6. The two graphs presented here is two subsets of the graph in Figure 5. Both graphs are presenting different patterns obtained from two sample intervals [350,550] and [1125,1325] respectively.

4-1- Visualization and Processing Algorithm

The visualization consists of a twostep algorithm, where the coloring follows a straightforward conversion from the pre-processed sound signal to a HSV (Hue, Saturation, Value) color model

$$\begin{aligned} h &= \frac{i_{nr}}{512} \\ s &= 1 \\ v &= 1 - \frac{j_{fft}}{j_{max}} \cdot 0.5. \end{aligned} \tag{1}$$

Where i is the sample index nr between [0,512] and $h \in [0,360]$. Saturation is set to a constant value 1 and the j_{fft} is the processed sound signal value divided on the max peak value, j_{max} mapping the total value v between [0.5,1].

The HSV color model produces a color representing the sound signal as shown in Figure 7.

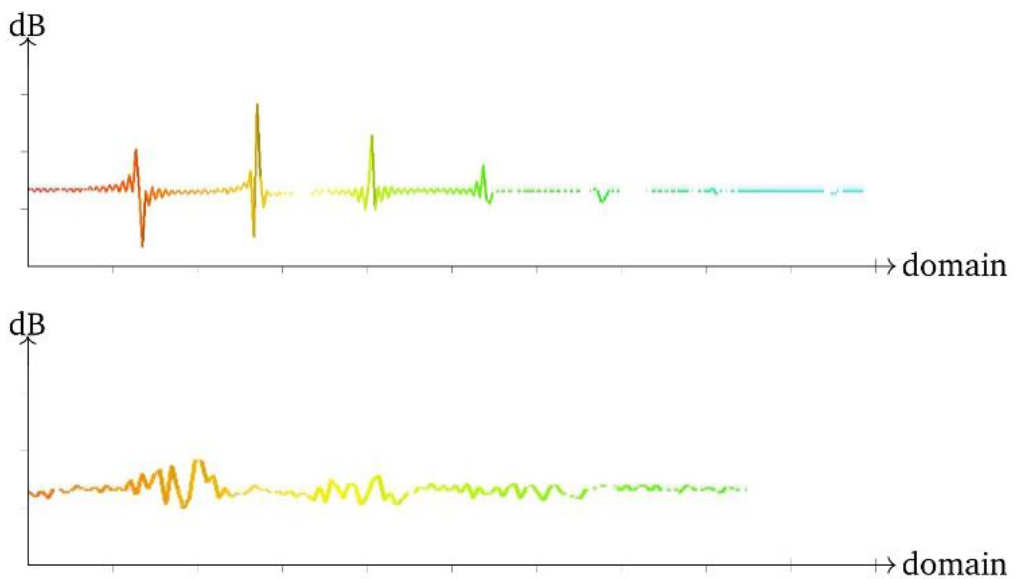


Figure 7. Sound signal after fft and coloring from Equation 1. Both figures represent the frequency domain separated into blocks. That is, the frequency from 0-12000hz is separated into 256 blocks after fft is performed. Figure on the top illustrates the signal.

The second step of the algorithm is drawing the movement pattern on a canvas where the colors are based on the combination of a frequency band analysis and time dependent intensity accumulation as follows:

$$\begin{aligned} \text{Induction} \rightarrow \text{Sound vs. time} &= (dB, t) \\ \text{Movement} \rightarrow \text{Accel + Gyro} &= (x, y, t) \end{aligned} \quad \left. \right\} (x, y, color). \quad (2)$$

The process of combining the frequency analysis with the movement pattern in the prototype application follows the evaluation scheme seen in Figure 8. The result is on the right-hand side where the sweeping motion is colored.

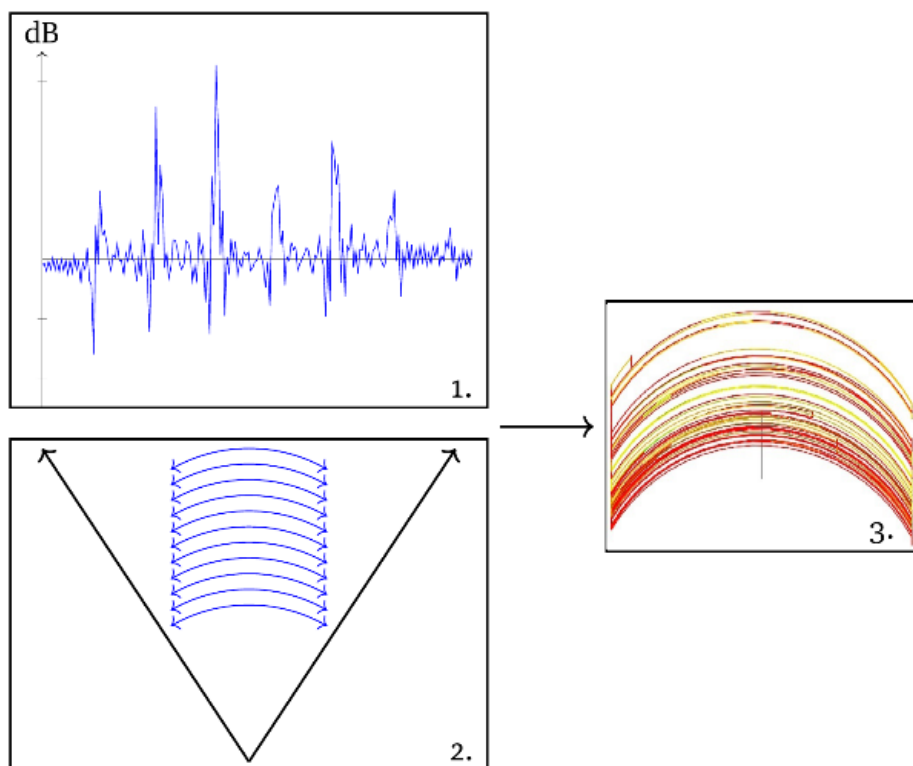


Figure 8. The illustration here provides a visual presentation of the algorithm, consisting of; 1. The frequency analysis from the signal acquired, 2. The movement pattern captured, 3. The resulting visualization using an algorithm with 1. and 2. as arguments generating a coloured trajectory following an arc.

4-2- Mapping and Deviation

The detector sweeping motion differs depending on the search state, where the angle changes as follows:

- General sweep → [80,120] $^{\circ}$.
- Targeted sweep → [40,80] $^{\circ}$.
- Pinpoint sweep → [10,40] $^{\circ}$.

Accuracy between screen dimension and ground measurement is calculated using curve length l_c (length of a complete sweep):

$$l_c = 2\pi \frac{\theta}{360^{\circ}}, \quad (3)$$

Where θ is the sweeping angle. A test case visualizing the three states can be seen in Figure 9.

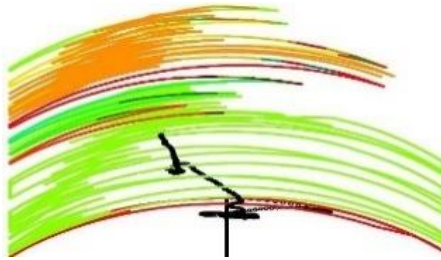


Figure 9. Visualization of the three sweep types Table 1. The sweep types are identified by the higher density of points in certain areas. Twice on the left bearing we see higher densities, which are a combination of targeted and pinpoint sweep. The colours are only present for visualization purposes.

Table 1. Curve length between the screen and ground using (3) with r fixed to 800px on the screen and 60cm on the ground

Sweep type	Screen l_c	Ground l_c
General 100 $^{\circ}$	1396px	104.7cm
Targeted 60 $^{\circ}$	837px	62.8cm
Pinpoint 25 $^{\circ}$	349px	26.2cm

The curve length ratio from Table 1 is $\frac{l_{c,screen}}{l_{c,ground}} = \frac{1396px}{104.7cm} = 13.33px/cm$. Since the mapping is a relative correlation between the physical space and the digital twin, see Figure 10, the ratio is an error estimate describing limitations of the current setup.

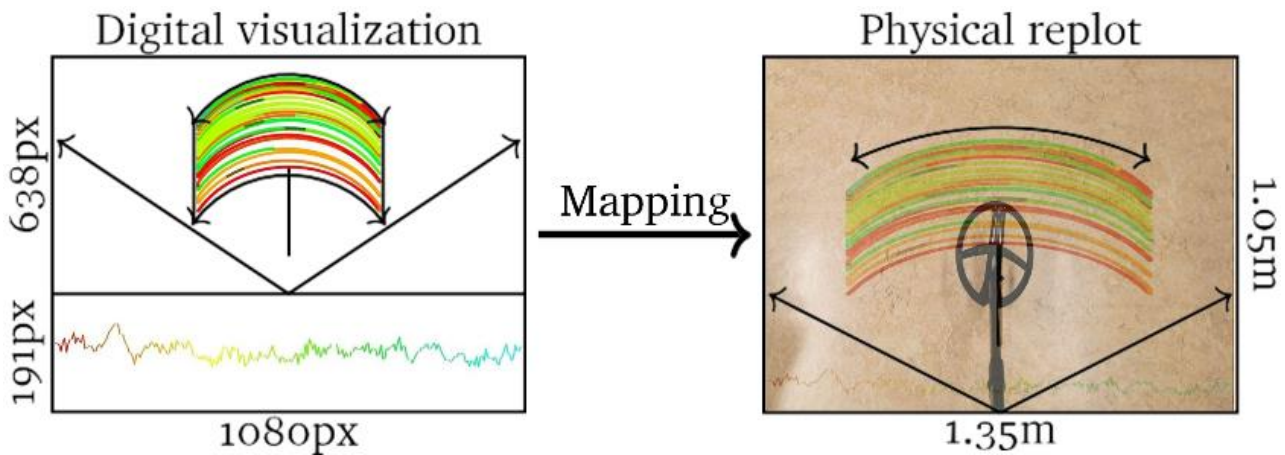


Figure 10. The mapping between screen drawing resolution and the physical ground size measured from the metal detector.

With other words, the obtainable accuracy is $1.3px$ for every $1mm$ on the ground using the current algorithm and mapping. Illustration of a test case where the average position values are visualized is shown in Figure 11. These positions show the tendency of the metal detector movement.

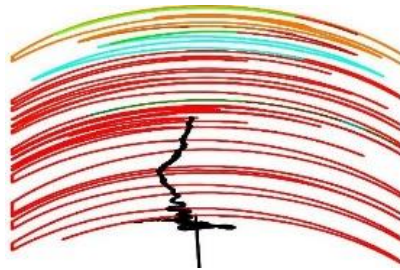


Figure 11. Visualization of a general sweeping motion with the average position values painted in black. The black trajectory is calculated using a moving average of the positions during a test case.

Next we calculate the standard deviation model as follows:

$$\sigma = \sqrt{\frac{1}{N} \sum_{i=1}^N (x_i - \bar{x})^2} \quad (4)$$

Where N is equal to the number of values in the total dataset, x_i is the value of the current index and \bar{x} is the average value of the total dataset.

The presented model is in this case used to estimate the deviation away from the average positions, hence, the graph in Figure 12 shows the tendencies around the average positions. Since the outward position is changing slowly based on the back and forth motion of the metal detector, it is similar to a linear development. The sweeping motion on the other hand is prone to higher values in the start, since we are in the general sweep phase. The curve is flattening out towards the area where we are pinpointing; hence, we have a higher point density.

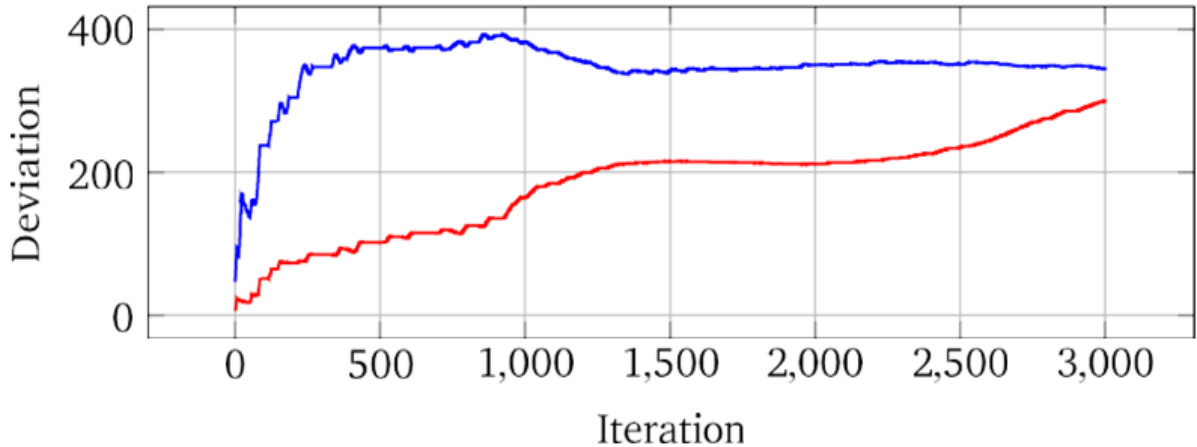


Figure 12. This graph is plotting the standard deviation in x-direction (blue) and y-direction (red). Since the deviation calculation is using a continuous average, calculating the deviation every time a movement is detected, we expect the x-direction to flatten out towards the centre of the motion and the y-direction to be close to linear.

4-3-Error Estimation

Precision on stability of sensor technology has been thoroughly researched in for instance [13-16]. However, the canvas is graphical approximation using position and coloring of pixels; therefor the visualization will introduce errors which are not considered in the present study. Figure 13 is illustrating the preliminary movement trajectory drawn on the canvas without any processing, i.e. smoothing and pathing.

There are limitations of the current framework, where for instance the sweeping motion is only valid when standing still and the trajectory calculated is only from the device itself.

The curve length mapping ratio was calculated ($13.33px/cm$) and Table 1 is estimating the obtainable accuracy of the current implementation. Stability of sensor technology, implementation of motion tracking and user movement restrictions will influence the precision of the total system.

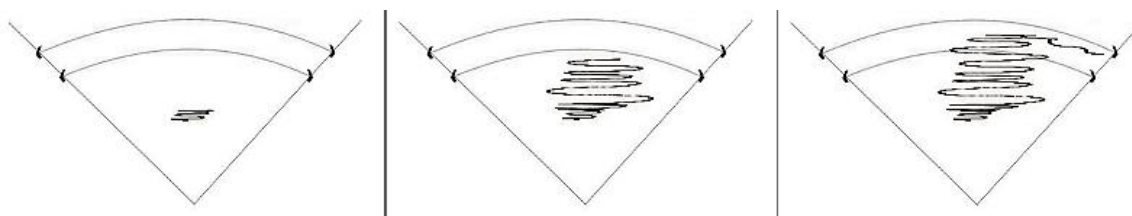


Figure 13. The preliminary movement testing with positions drawn on a canvas for visualization purposes.

When performing a sweep, such as the data shown in Figure 14, the three states have different error ratios and calculating the standard deviation shown in Figure 12, we are able to trace where the error ratio is at a maximum. The general sweep is going to have the biggest deviation, and by narrowing the sweep angle we achieve increased accuracy. The deviation is showing a higher precision (less turbulent) when the system is run longer, and we are using the pinpointing sweep state. Since the values of sweeping is higher than the back and forth motion, the y-axis deviation for back and forth motion is close to linear.

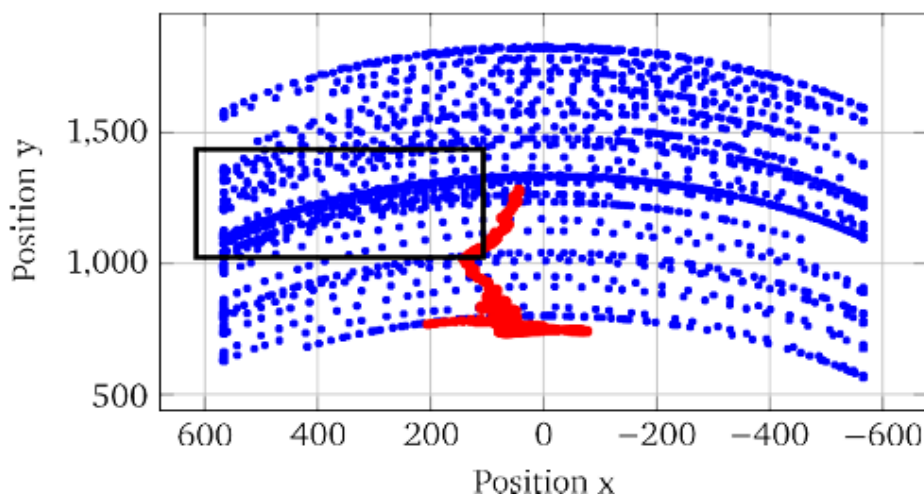


Figure 14. The graph plots the positions before using the visualization algorithm, that is, we show the movement intensity by point density. The red dots are the average values. The tendency towards the left on the red dots is explained by the greater amount of positions toward the left area, shown in the black rectangle.

5- Conclusion

Starting the development of a prototype application and implementing a multi-sensor system using the built-in sensor in a mobile phone, such as accelerometer, gyroscope, sound (microphone) and a metal detector, requires some extensive testing where we measure the outputs of the non-calibrated sensors. This is done in order to both properly calibrate the sensors, but also to know what to expect and include in the prototype application.

Since the signal and component magnitudes can differ and the receiving signal can be weak depending on the depth to the object, a thorough analysis is required. The coloring scheme used for visualization purposes uses a signal that needs pre-processing, e.g., filtering or smoothing.

We present a custom setup using a metal detector with an off-the-shelf smartphone creating a digital twin.

We have created a tool for interactively modelling the inputs and visualize the information, and the canvas drawing is analogous to sketching indentation clues on a paper using an object beneath.

5-1-Future Comments

For future development the signal wave lengths should be analyzed and using the signal amplitude, a better accuracy pinpointing the location of an object should be obtainable.

The current implementation does not allow for the user change orientation during a sweep, and for future reference, the solution for this problem could be in generating reference points on the ground. The reference points can generate a stable ground-frame, which enables the user to rotate freely and change orientation during a recording.

6- Conflict of Interest

The author declares that there is no conflict of interests regarding the publication of this manuscript. In addition, the ethical issues, including plagiarism, informed consent, misconduct, data fabrication and/or falsification, double publication and/or submission, and redundancies have been completely observed by the authors.

7- References

- [1] Stankevich, Evgeny, Ilya Paramonov, and Ivan Timofeev. "Mobile Phone Sensors in Health Applications." 2012 12th Conference of Open Innovations Association (FRUCT) (November 2012). doi:10.23919/fruct.2012.8122097.
- [2] Angelov, George Vasilev, Dimitar Petrov Nikolakov, Ivelina Nikolaeva Ruskova, Elitsa Emilova Gieva, and Maria Liubomirova Spasova. "Healthcare Sensing and Monitoring." Enhanced Living Environments (2019): 226–262. doi:10.1007/978-3-030-10752-9_10.
- [3] Bonato, Paolo. "Advances in wearable technology and applications in physical medicine and rehabilitation," Journal of NeuroEngineering and Rehabilitation 2, no. 1 (2005): 2. doi:10.1186/1743-0003-2-2.
- [4] Cho, Soojin, Hongki Jo, Shinae Jang, Jongwoong Park, Hyung-Jo Jung, Chung-Bang Yun, Billie F. Jr. Spencer, and Ju-Won Seo. "Structural Health Monitoring of a Cable-Stayed Bridge Using Wireless Smart Sensor Technology: Data Analyses." Smart Structures and Systems 6, no. 5_6 (July 25, 2010): 461–480. doi:10.12989/sss.2010.6.5_6.461.
- [5] Arognam, Gobinath, Nadarajah Manivannan, and David Harrison. "Review on Wearable Technology Sensors Used in Consumer Sport Applications." Sensors 19, no. 9 (April 28, 2019): 1983. doi:10.3390/s19091983.
- [6] Trafialek, Joanna, Sylwia Kaczmarek, and Wojciech Kolanowski. "The Risk Analysis of Metallic Foreign Bodies in Food Products." Journal of Food Quality 39, no. 4 (February 2, 2016): 398–407. doi:10.1111/jfq.12193.
- [7] Hamzah, Hazwani Binte, Vigil James, Suraj Manickam, and Sashikumar Ganapathy. "Handheld Metal Detector for Metallic Foreign Body Ingestion in Pediatric Emergency." The Indian Journal of Pediatrics 85, no. 8 (January 4, 2018): 618–624. doi:10.1007/s12098-017-2552-5.
- [8] Bhattacharyya, Ananya. "Bluetooth Controlled Metal Detector Robot." ADBU Journal of Electrical and Electronics Engineering (AJEEE) 1, no. 1 (2017): 1-5.
- [9] Candy, Bruce. "Metal Detector Basics and Theory." Minelab Pty Ltd. Technical Report (2007).
- [10] G. Watson, "Right Hand Rule for Cross Products," 1998. Available online: <http://www.physics.udel.edu/~watson/phys345/Fall1998/class/1-right-hand-rule.html> (accessed 22 March 2020).
- [11] X. P. Detectors, "XP Metal Detectors - A new adventure," 2020. Available online: <https://www.xpmetaldetectors.com/metal-detector/deus/> (accessed 22 March 2020).
- [12] Celestron, "Optics and special mounts," 2020. Available online: <https://www.celestron.com/products/nexyz-3-axis-universal-smartphone-adapter> (accessed 22 March 2020).
- [13] Zhizhong Ma, Yuansong Qiao, B. Lee, and E. Fallon. "Experimental Evaluation of Mobile Phone Sensors." 24th IET Irish Signals and Systems Conference (ISSC 2013) (2013). doi:10.1049/ic.2013.0047.
- [14] Du, J., C. Gerdtsman, and Maria Lindén. "Signal Processing Algorithms for Position Measurement with MEMS-Based Accelerometer." 16th Nordic-Baltic Conference on Biomedical Engineering (2015): 36–39. doi:10.1007/978-3-319-12967-9_10.
- [15] F. F. U. Shala and K. Klonowska, "Indoor Positioning using Sensor-fusion in Android Devices," 15 Credits Master work in embedded systems, 2011.
- [16] J. D. H. M. Kok and T. B. Schon, "Using Intertial Sensors for Position and Orientation Estimation," Foundations and Trends in Signal Processing, pp. 1-153, 2017.